Numerical spectral synthesis of breather gas for the focusing nonlinear Schrödinger equation

Giacomo Roberti , Gennady El , Alexander Tovbis, François Copie , Pierre Suret , and Stéphane Randoux , horthumbria University, Newcastle upon Tyne NE1 8ST, United Kingdom Department of Mathematics, University of Central Florida, Orlando, Florida 32816, USA Univ. Lille, CNRS, UMR 8523 PhLAM Physique des Lasers Atomes et Molécules, F-59 000 Lille, France

(Received 15 January 2021; accepted 16 March 2021; published 9 April 2021)

We numerically realize a breather gas for the focusing nonlinear Schrödinger equation. This is done by building a random ensemble of $N \sim 50$ breathers via the Darboux transform recursive scheme in high-precision arithmetics. Three types of breather gases are synthesized according to the three prototypical spectral configurations corresponding the Akhmediev, Kuznetsov-Ma, and Peregrine breathers as elementary quasiparticles of the respective gases. The interaction properties of the constructed breather gases are investigated by propagating through them a "trial" generic (Tajiri-Watanabe) breather and comparing the mean propagation velocity with the predictions of the recently developed spectral kinetic theory [El and Tovbis, Phys. Rev. E 101, 052207 (2020)].

DOI: 10.1103/PhysRevE.103.042205

I. INTRODUCTION

The study of nonlinear random waves in physical systems well described at leading order by the so-called integrable equations, such as the Korteweg-de Vries (KdV) or nonlinear Schrödinger (NLS) equations, has recently become the topic of intense research in several areas of nonlinear physics, notably in oceanography and nonlinear optics. This interest is motivated by the complexity of many natural or experimentally observed nonlinear wave phenomena often requiring a statistical description even though the underlying physical model is in principle amenable to the well-established mathematical techniques of integrable system theory such as the inverse scattering transform (IST) or finite-gap theory [1]. An intriguing interplay between integrability and randomness in such systems is nowadays associated with the concept of integrable turbulence introduced by Zakharov in [2]. The integrable turbulence framework is particularly pertinent to the description of modulationally unstable systems whose solutions, under the effect of random noise, can exhibit highly complex spatiotemporal dynamics that is adequately described in terms of turbulence theory concepts, such as the distribution functions, ensemble averages, and correlations.

Solitons and breathers are the elementary quasiparticles of nonlinear wave fields in integrable systems which can form ordered coherent structures such as modulated soliton trains and dispersive shock waves [3,4], superregular breathers [5,6], or breather molecules [7]. Furthermore, solitons and breathers can form *irregular* structures or statistical ensembles that can be viewed as soliton and breather gases. The nonlinear wave field in such integrable gases represents a particular case of integrable turbulence [2,8–13]. The observations of soliton and breather gases in the ocean have been reported in Refs. [14–17]. Recent laboratory experiments on

the generation of shallow-water and deep-water soliton gases were reported in Refs. [18,19], respectively. It has also been demonstrated that the soliton gas dynamics in the focusing NLS equation provides a remarkably good description of the statistical properties of the nonlinear stage of spontaneous modulational instability [20].

An analytical description of soliton gases was initiated by Zakharov in Ref. [21], where a spectral kinetic equation for KdV solitons was derived using an IST-based phenomenological procedure of computing an effective adjustment to a soliton's velocity in a rarefied gas due to its collisions with other solitons, accompanied by appropriate phase shifts. Zakharov's kinetic equation for KdV soliton has been generalized to the case of a dense gas in Ref. [22] using the spectral finite-gap theory. Within this theory, a uniform (equilibrium) soliton gas is modeled by a special infinite-phase thermodynamic-type limit of finite-gap KdV solutions. The kinetic description of the nonequilibrium soliton gas is then enabled by considering the same thermodynamic limit for the associated modulation (Whitham) equations. The resulting kinetic equation describes the evolution of the density of states defined as the density function in the spectral (IST) phase plane of soliton gas. The spectral construction of the KdV soliton gas in Ref. [22] was generalized to the soliton gas of the focusing NLS equation (NLSE) in Refs. [23,24]. The latter work [24] provides also the spectral kinetic description of a breather gas (BG), which is the main subject of the present work.

An isolated generic breather can be broadly viewed as a soliton on the plane-wave (or finite) background. The one-dimensional (1D) NLSE supports a large family of breather solutions that have attracted particular interest due to their explicit analytic nature and the potential for modeling the rogue wave events in the ocean and in nonlinear optical fibers [25–29]. Three types of breathers, namely, the Akhmediev breather (AB), the Kuznetsov-Ma (KM) breather, and the Peregrine soliton (PS) have aroused significant research

^{*}stephane.randoux@univ-lille.fr

interest (see [30-35] and references therein). The AB, KM breather, and PS represent special cases of a generic breather called the Tajiri-Watanabe (TW) breather [36]. The simplest example of a breather gas can be viewed as an infinite random ensemble of TW breathers [24]. By manipulating the spectral parameters, the TW breather gas can be reduced to the AB, KM, and PS gases as well as to the fundamental soliton gas. The latter is achieved by vanishing the plane-wave background of the TW breather gas [24].

The present paper has two goals: (i) numerical realization of a breather gas and (ii) verification of the spectral theory of a breather gas developed in Ref. [24]. Numerical realization of a breather gas as a large ensemble of TW breathers with prescribed parameters represents a challenging problem. Numerical methods for the construction of breather solutions of the 1D NLSE suffer from accuracy problems that prevent the numerical synthesis of breathers of order $N \gtrsim 5$ [37,38]. In the context of soliton gases, this latter difficulty has been resolved recently by Gelash and Agafontsev [39] via the application of the so-called dressing method combined with high-precision numerical computations. In this paper we extend the algorithm of [39] to numerically realize various breather gases and verify some predictions of the spectral kinetic theory of [24]. In particular, we demonstrate that random ensembles of $N \sim 50$ breathers can be built via the Darboux transform recursive scheme in high-precision arithmetics. This represents an improvement of an order of magnitude compared to the results reported in previous numerical works. In addition, we show that the construction method can be used to provide evidence of the space-time evolution of the generated breather gases. This feature cannot be achieved by using direct numerical simulations of the 1D NLSE due to the inevitable presence of modulational instability that quickly disintegrates the plane-wave background.

The paper is organized as follows. In Sec. II we present the algorithm of the spectral synthesis of a breather gas using the Darboux transform. This algorithm is then realized numerically using the high-precision arithmetics. In Sec. III we numerically study the interactions in breather gases and compare the results of the numerical simulations with the theoretical predictions of the breather gas kinetic theory of Ref. [24]. Specifically, we consider the propagation of the "trial" breather through a homogeneous breather gas for three prototypical configurations: Akhmediev, Kuznetsov-Ma, and Peregrine gases. The study of interaction in the gas of Akhmediev breathers has revealed some special features that have required further development of the theory of Ref. [24]. The Appendix provides the identification of the interaction kernel in the breather gas with the position shift formula in twobreather collisions, obtained in earlier works.

II. NONLINEAR SPECTRAL SYNTHESIS OF BREATHER GASES

A. Overview of soliton and breather ensembles in the 1D NLSE

We consider the integrable 1D NLSE in the form

$$i\psi_t + \psi_{xx} + 2|\psi|^2 \psi = 0, \tag{1}$$

where $\psi(x,t)$ represents the complex envelope of the wave field that evolves in space x and time t. In the IST method, the 1D NLSE (1) is represented as a compatibility condition of two linear equations [1,40]

$$\Phi_{x} = \begin{pmatrix} -i\lambda & \psi \\ -\psi^{*} & i\lambda \end{pmatrix} \Phi, \tag{2}$$

$$\Phi_{x} = \begin{pmatrix} -i\lambda & \psi \\ -\psi^{*} & i\lambda \end{pmatrix} \Phi, \qquad (2)$$

$$\Phi_{t} = \begin{pmatrix} -2i\lambda^{2} + i|\psi|^{2} & i\psi_{x} + 2\lambda\psi \\ i\psi_{x}^{*} - 2\lambda\psi^{*} & 2i\lambda^{2} - i|\psi|^{2} \end{pmatrix} \Phi, \qquad (3)$$

where λ is a (time-independent) complex spectral parameter and $\Phi(x, t, \lambda) = [r(x, t, \lambda), s(x, t, \lambda)]^T$ is a column vector. The spatial linear operator (2) and the temporal linear operator (3) form the Lax pair of Eq. (1). For a given potential $\psi(x,t)$ the problem of finding the scattering data $\sigma[\psi]$ (also sometimes called the IST spectrum) and the corresponding scattering solution Φ specified by the spatial equation (2) is called the Zakharov-Shabat (ZS) scattering problem [41]. The ZS scattering problem is formally analogous to calculating the Fourier coefficients in the Fourier theory of linear systems; hence the term nonlinear Fourier transform is often used in the context of telecommunication system research, particularly in the context of periodic boundary conditions [42–44].

For spatially localized potentials ψ such that $\psi(x,t) \to 0$ as $|x| \to \infty$, the complex eigenvalues λ are generally presented by a finite number of discrete points with $Im(\lambda) \neq 0$ (discrete spectrum) and the real line $\lambda \in \mathbb{R}$ (continuous spectrum). The scattering data $\sigma(\psi)$ consist of a set of N discrete eigenvalues λ_n (n = 1, ..., N), a set of N norming constants C_n for each λ_n , and the so-called reflection coefficient $\rho(\xi)$,

$$\sigma(\psi) = \{ \rho(\xi); \lambda_n, C_n \}, \tag{4}$$

where $\xi \in \mathbb{R}$ denotes the continuous spectrum component. In this setting where the wave field ψ exists on a zero background, the discrete part of the IST spectrum is related to the soliton content of the wave field whereas the continuous part of the IST spectrum is related to the nonlinear dispersive radiation [41].

A special class of (reflectionless) solutions of Eq. (1), the N-soliton solutions (NSSs), exhibits only a discrete spectrum $[\rho(\xi) = 0]$ consisting of N complex-valued eigenvalues λ_n , n = 1, ..., N, and N associated complex-valued norming constants. The IST formalism has been extensively applied to examine the processes of interaction, collision, and synchronization in NSSs (see, e.g., Refs. [41,45]). The numerical synthesis of NSSs can be achieved in standard computer simulations (double precision, 16 digits) up to $N \sim 10$ [39]. On the other hand, the numerical synthesis of NSSs with N large represents a challenging problem that has been resolved only recently [39]. Combining the so-called dressing method and numerical calculations made using high numerical precision (a 100-digit precision is typically necessary for the synthesis of NSSs with $N \sim 100$), the numerical synthesis of soliton gases (SGs), i.e., large ensembles of NSSs characterized by a given spectral distribution, has been demonstrated in Ref. [39]. The opportunity to synthesize numerically large soliton ensembles has opened the way to the experimental generation of strongly nonlinear wave fields with a pure solitonic content. In particular, recent experiments made in a one-dimensional water tank with deep-water surface gravity waves have revealed that the controlled synthesis of dense SGs can be achieved in hydrodynamics [19]. Moreover, it also has been recently shown that the so-called bound-state SGs provide a model that describes well the nonlinear stage of the noise-induced modulation instability [20].

In addition to the soliton solutions existing on a zero background, the focusing NLS equation (1) admits a large variety of solutions existing on a nonzero (plane-wave) background. The IST theory for the focusing nonlinear Schrödinger equation with nonzero boundary conditions (NZBCs) at infinity has been reported in Refs. [46–48]. As in the IST with zero boundary conditions, the scattering data $\sigma[\psi]$ in the IST with NZBCs consist of a set of N discrete complex-valued eigenvalues λ_n , a set of N associated norming constants C_n , and the reflection coefficient $\rho(\lambda)$. In the IST with NZBCs, the continuous spectrum does not exist on the real axis \mathbb{R} but on $\mathbb{R} \cup [-iq_0, iq_0]$, where $q_0 > 0$ represents the amplitude of the plane-wave background [46,47].

The focusing NLS equation with NZBCs possesses a rich family of purely solitonic solutions [reflectionless potentials, $\rho(\lambda) = 0$] named breathers or sometimes solitons on a finite background. The generic "elementary" breather parametrized by one single complex-valued eigenvalue (N = 1) in the framework of the IST with NZBCs is the so-called Tajiri-Watanabe breather [36]. This elementary solution reduces under certain limits to the solutions found over the years by Kuznetsov [30], Ma [48], Peregrine [31], and Akhmediev [32]. Using the dressing method, Zakharov and Gelash constructed a class of two-soliton solutions on a finite background, termed superregular breathers and corresponding to small initial perturbations of a constant background [49]. This was generalized to several pairs of breathers in Refs. [5.50]. Note that most of these breather solutions of Eq. (1) have been experimentally realized in hydrodynamics and in optics [6,7,33,34,51-56] but also recently with matter waves [57].

B. Darboux transform-based synthesis of breather gases

The recent interest in studying the breather solutions of various kinds has been fueled by rogue-wave research (see, e.g., [58] and references therein). The prototypical rogue-wave solutions represent coherent structures of large amplitude, strongly localized in both space and time, on an otherwise quiescent background [25,27,38,59–65]. In this context the Darboux transform has been extensively used as a reliable method to generate higher-order breather solutions of Eq. (1), i.e., reflectionless solutions of the focusing 1D NLSE with NZBCs [37,66–69]. Note that the Darboux transform is now also used in the context of nonlinear eigenvalue communication to build ordered soliton ensembles used to carry out the transmission of information in fiber optic communication links [43,44,70].

The Darboux method is a recursive transformation scheme where a "seeding solution" of the focusing 1D NLSE is used as a building block for the construction of a higher-order solution through the addition of one discrete eigenvalue. Here we give a brief review of the Darboux transform method used for the generation of higher-order breathers. We largely follow the exposition given in Refs. [38,71], but other important references where this method is described and used are Refs. [37,66–69].

In the IST for the 1D NLSE with NZBCs, the seeding solution commonly used at the first step of the recursive process of constructing a higher-order breather solution is the plane-wave solution of Eq. (1) with unit amplitude, i.e., $\psi_0(x,t) = e^{2it}$. The first-order (Tajiri-Watanabe) breather $\psi_1(x,t)$ parametrized by the complex eigenvalue λ_1 is obtained by

$$\psi_1(x,t) = \psi_0(x,t) + \frac{2(\lambda_1^* - \lambda_1)s_{1,1}r_{11}^*}{|r_{1,1}|^2 + |s_{1,1}|^2}.$$
 (5)

The functions $r_{1,1}(x, t)$ and $s_{1,1}(x, t)$ in Eq. (5) are obtained by setting j = 1 in the expressions

$$r_{1,j}(x,t) = 2ie^{-it}\sin(A_j),$$

 $s_{1,j}(x,t) = 2e^{it}\cos(B_j),$ (6)

where A_i and B_i are given by

$$A_{j} = \frac{1}{2} \left[\arccos\left(\frac{\kappa_{j}}{2}\right) + (x - x_{j})\kappa_{j} - \frac{\pi}{2} \right] + (t - t_{j})\kappa_{j}\lambda_{j},$$

$$B_{j} = \frac{1}{2} \left[-\arccos\left(\frac{\kappa_{j}}{2}\right) + (x - x_{j})\kappa_{j} - \frac{\pi}{2} \right] + (t - t_{j})\kappa_{j}\lambda_{j},$$
(7)

with $\kappa_j = 2\sqrt{1 + \lambda_j^2}$. The parameters (x_j, t_j) are connected with the complex norming constants C_j in the IST with NZBCs [37]. The first-order breather $\psi_1(x, t)$ is parametrized by the complex eigenvalue λ_1 and by the two real parameters x_1 and t_1 . Once the first-order breather ψ_1 is constructed using Eqs. (5)–(7), breather solutions of order $n \ge 2$ can be recursively generated by using

$$\psi_n(x,t) = \psi_{n-1}(x,t) + \frac{2(\lambda_n^* - \lambda_n)s_{n,1}r_{n,1}^*}{|r_{n,1}|^2 + |s_{n,1}|^2},$$
 (8)

with

$$r_{n,p} = [(\lambda_{n-1}^* - \lambda_{n-1})s_{n-1,1}^* r_{n-1,1} s_{n-1,p+1} + (\lambda_{p+n-1} - \lambda_{n-1})|r_{n-1,1}|^2 r_{n-1,p+1} + (\lambda_{p+n-1} - \lambda_{n-1}^*)|s_{n-1,1}|^2 r_{n-1,p+1}] \times (|r_{n-1,1}|^2 + |s_{n-1,1}|^2)^{-1},$$

$$(9)$$

$$s_{n,p} = [(\lambda_{n-1}^* - \lambda_{n-1})s_{n-1,1} r_{n-1,1}^* r_{n-1,p+1} + (\lambda_{p+n-1} - \lambda_{n-1}^*)|s_{n-1,1}|^2 s_{n-1,p+1} + (\lambda_{p+n-1} - \lambda_{n-1}^*)|r_{n-1,1}|^2 s_{n-1,p+1}] \times (|r_{n-1,1}|^2 + |s_{n-1,1}|^2)^{-1}.$$

$$(10)$$

Despite the efficiency of the Darboux method for the construction of high-order breather solutions of Eq. (1), its practical implementation in numerics suffers from the same type of issues as those previously mentioned for the numerical construction of NSSs. As noted in Refs. [37,38], problems of numerical accuracy may prevent the numerical synthesis of breathers of order $N \gtrsim 5$. In this paper we show that this limit can be overcome by the implementation of the same strategy as the one used to build NSSs with N large [39]. Implementing the Darboux recursive scheme in high-precision arithmetics using the BOOST C++ multiple precision library, we show that breather solutions of Eq. (1)

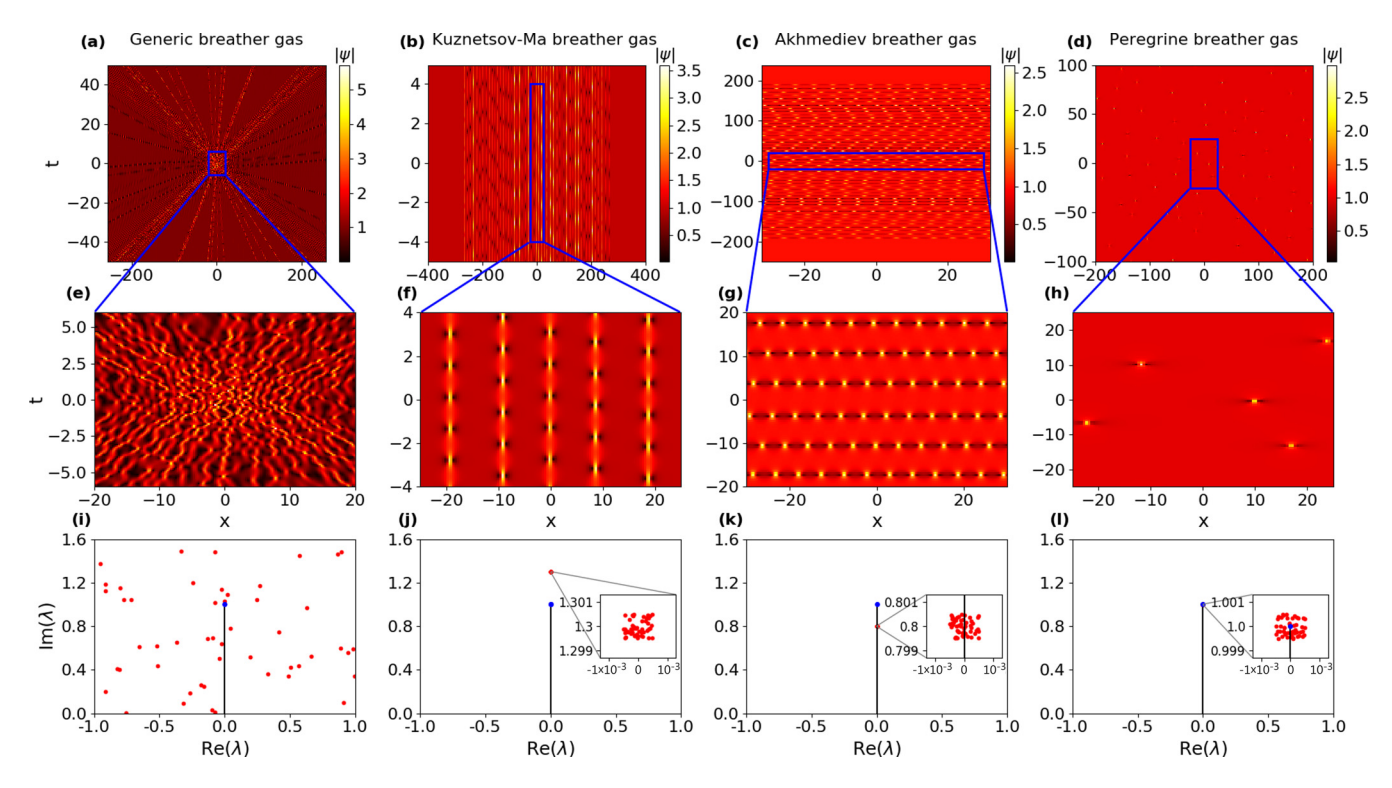


FIG. 1. Numerical synthesis of (a), (e), and (i) a generic BG (column 1) and of three single-component BGs (columns 2–4): (b), (f), and (j) a KMBG; (c), (g), and (k) an ABG; and (d), (h), and (i) a PS BG. The four BGs are parametrized by N = 50 complex eigenvalues λ_n [see (i)–(l)]. (a)–(d) Space-time evolution of the BGs. (e)–(h) Enlarged view of some restricted region of the (x, t) plane. (i)–(l) Spectral portraits of each BG with the vertical line between 0 and +i being the branch cut associated with the plane-wave background. Each point in the upper complex plane in (i)–(l) represents a discrete eigenvalue in the IST problem with NZBCs. The eigenvalues parametrizing the single-component BGs are densely placed in a small square region which is centered around a point λ_0 of the imaginary vertical axis and which is greatly enlarged in the insets shown in (j)–(l). The x_j are uniformly distributed in the range [-1, 1] for (a) the generic gas and (d) the Peregrine gas, while they are uniformly distributed in the range [-32, 32] for (b) the KM gas and (c) the AB gas.

can be synthesized up to order $N \sim 50$. As will be shown in detail in Sec. III, this provides a numerical tool that enables one to verify the results of the spectral theory of breather gases recently developed in Ref. [24].

Figure 1(a) shows the space-time evolution of a generic BG, i.e., a breather solution of Eq. (1) of order N = 50with random spectral characteristics. The amplitude of the plane-wave background is unity $(q_0 = |\psi_0| = 1)$ and the 50 complex-valued eigenvalues λ_i (j = 1-50) parametrizing the BG are randomly distributed within some rectangular region of the upper complex plane [see Fig. 1(i)]. The parameters t_i are set equal to zero $(t_i = 0 \,\forall j)$ and the randomness of the gas is achieved by uniformly distributing the x_i in some interval centered around $x_0 = 0$. Note that the vertical line between 0 and +i in Fig. 1(i) represents the so-called branch cut associated with the plane-wave background in the IST formalism of the 1D NLSE with a nonzero background (see, e.g., [24,35,46,47]). Figure 1(a) reveals that the space-time dynamics of the generic BG synthesized in numerical simulations is highly complicated. In particular, breathers cannot be individualized due to their strong overlap and interaction. Note also that the maximum amplitude reached locally in space and time by the incoherent breather ensemble of Fig. 1(a) does not exceed \sim 5.5, which demonstrates that the multiple breathers are far from a synchronization state that would eventually produce isolated rogue waves of large amplitude [72,73].

We emphasize that BGs shown in the space-time plots of Fig. 1 are not obtained from a numerical simulation of Eq. (1). Taking a BG generated at a given time t_0 using the Darboux method and using this wave field as the initial condition in a numerical simulation of Eq. (1), we observe that modulation instability quickly disintegrates the plane-wave background by amplifying the numerical noise inherent to any pseudospectral (split-step-like) method commonly used for the numerical integration of the 1D NLSE. On the other hand, space-time plots reported in Fig. 1 are obtained from a pure spectral (IST) construction based on the Darboux recursive method which has been implemented in computer simulations made with high numerical precision. Starting from an ensemble of N complex eigenvalues λ_i and N coordinates (x_i, t_i) , the BG is synthesized at time t using the Darboux machinery [Eqs. (5)–(10)]. A 100-digit precision is typically necessary to synthesize a BG parametrized by an ensemble of $N \sim 50$ eigenvalues. The space-time plots shown in Fig. 1 are obtained by reiterating the same synthesis at different values of time t. Our numerically synthesized solutions can be validated by computing the discrete Zakharov-Shabat spectrum (using, for instance, the Fourier collocation method [35,41]) at different moments of time to verify that the obtained discrete eigenvalues are indeed the same as the ones specified for the construction of the BG under consideration.

The central concept in the theory of SGs and BGs is the density of states (DOS) [74] which represents the distribution function $u(\lambda, x, t)$ in the spectral phase space. In the context of the 1D NLSE (1), the DOS $u(\lambda, x, t)$, where $\lambda = \beta + i\gamma$, is defined such that $ud\beta d\gamma dx$ is the number of breather states with complex spectral parameter $\lambda \in [\beta, \beta + d\beta] \times [\gamma, \gamma + d\gamma]$ contained in a portion of the BG within a spatial interval [x, x + dx] at time t.

One-component BGs have been defined in Ref. [24] as being characterized by a DOS in the form of the Dirac δ distribution, i.e., $u(\lambda) = w\delta(\lambda - \lambda_0)$, where w > 0 represents the mass of the δ distribution which is centered around one specific point λ_0 in the complex spectral plane. Figures 1(b)–1(d) and 1(f)–1(h) display the space-time evolutions together with the spectral portraits [Figs. 1(j)–1(l)] typifying some one-component BGs of particular interest.

For the Kuznetsov-Ma BG (KMBG), the spectral portrait consists of the branch cut (associated with the plane-wave background of unity amplitude) and a dense set of N = 50 spectral points randomly placed in a small square region of width $\delta = 10^{-3}$ centered around $\lambda_0 = 1.3i$, as shown in Fig. 1(j). Figure 1(b) shows that the KMBG is a dense ensemble of individual KM breathers, all having a zero velocity in the (x, t) plane. In contrast to Fig. 1(a), each KM breather inside the BG can be individualized and the BG follows the same periodic time evolution where the time period is fully determined by $\text{Im}(\lambda_0)$. The randomness in the one-component KMBG can be seen from the random distance between individual KM breathers and their random initial phase [see Fig. 1(f)].

The Akhmediev BG (ABG) is characterized by the same distribution of the spectrum λ as the KMBG except that the point λ_0 around which the multiple discrete eigenvalues are accumulated is now placed inside the branch cut associated with the plane-wave background [see Fig. 1(k)], where $\lambda_0 = +0.8i$. As a result, the ABG is more naturally characterized by the *spectral flux density*, the temporal counterpart of the DOS. As shown in Fig. 1(c), the ABG consists of a random series of individual ABs having identical spatial period, which is fully determined by $\text{Im}(\lambda_0)$. Similarly to the KMBG, the randomness in the one-component ABG can be seen from the random time separation between individual Akhmediev breathers and their random relative phases [see Fig. 1(g)].

It must be mentioned that the density (spatial or temporal) of the AB or KM breather gases cannot be made arbitrarily large: There is a configuration termed breather condensate [24] corresponding to a critically dense breather gas, similar to a soliton condensate numerically realized in Ref. [20].

It is well known that the Peregrine breather can be obtained as the spatial and temporal infinite-period limits of Akhmediev and Kuznetsov-Ma breathers, respectively [68,71]. In the spectral (IST) domain, the Peregrine breather is obtained by placing the eigenvalue parametrizing a first-order breather solution of Eq. (1) exactly at the end point +i of the branch cut associated with the plane-wave background of unit amplitude [35]. Following the same approach, the one-component Peregrine BG (PBG) is obtained by accumulating a large number of discrete eigenvalues in a small area surrounding the end point of the branch cut [see Fig. 1(1)]. As shown in Figs. 1(d) and 1(h), the PBG represents a collection of individual and

identical Peregrine breathers that are randomly positioned in space and time.

While the PG synthesized in our work represents a highorder breather solution of Eq. (1), this solution contrasts with the high-order breather solutions considered previously because it is intrinsically of a random nature. The localized breather solutions of high order that have been considered in previous works (see, e.g., Refs. [38,62,64,71]) have been arranged in regular patterns with well-organized geometrical shapes because they represented synchronized states having no degree of randomness. In contrast, in the construction plotted in Figs. 1(d) and 1(h), the parameters x_i are randomly and uniformly distributed over [-1, +1], which implies that each individual Peregrine breather in the PG has a random position in the (x, t) plane. We also mention that the solitonic eigenvalues in our numerical construction are clustered (also randomly) in close proximity to the end points of the spectral branch cut, so the individual Peregrine solitons in the PG are realized in our synthesis approximately, with the accuracy determined by the closeness of the solitonic eigenvalues to the end points of the branch cut.

III. INTERACTIONS IN BREATHER GASES: COMPARISON BETWEEN NUMERICAL EXPERIMENTS AND SPECTRAL THEORY

The analytical theory of BGs was introduced and developed in Ref. [24]. It was shown that spatially nonhomogeneous BGs are described by a kinetic equation formed by a transport equation for the slowly varying DOS $u(\lambda, x, t)$ and the integral equation of state relating the gas velocity to the DOS. In this section we show that some predictions of the spectral theory of BGs can be verified in simulations involving BGs that have been numerically synthesized using the methodology described in Sec. II B. In Sec. III A we provide the key elements of spectral theory of BGs that are relevant for the comparison between theoretical and numerical results. In Sec. III B we examine the collision between one trial soliton and various single-component BGs.

A. Analytical results from the spectral theory of breather gases

The nonlinear spectral theory of SGs and BGs for the focusing 1D NLSE developed in Ref. [24] provides a full set of equations characterizing the macroscopic spectral dynamics in a spatially nonhomogeneous BG. An important result of the theory is the so-called equation of state which provides the mathematical expression of the modification of the mean velocity of a "tracer" breather due to its interaction with other breathers in the gas.

The group velocity [in the (x,t) plane] of a first-order (TW) breather parametrized by the complex eigenvalue $\lambda \equiv \eta$ (we will use in this section the latter notation for the spectral parameter to be consistent with notation of Ref. [24] and previous works on the spectral kinetic theory) is given by

$$s_0(\eta) = -2 \frac{\text{Im}[\eta R_0(\eta)]}{\text{Im}[R_0(\eta)]},$$
 (11)

where $R_0(z) = \sqrt{z^2 - \delta_0^2}$, with δ_0 the end point of the branch cut corresponding to the plane wave $(\delta_0 = i$ for the plane

wave of unit amplitude considered in all the numerical simulations reported in this paper). It is not difficult to see that, if $\eta \in i\mathbb{R} \setminus [-i, i]$ (KM breather), then $s_0(\eta) = 0$, while if $\eta \in (-i, i)$ (AB), then $s_0(\eta) = \pm \infty$ depending on the way the limit $\text{Re}(\eta) \to 0$ in Eq. (11) is taken (either from the left or right side of the branch cut).

As shown in Ref. [24], the equation of state of a BG reads

$$s(\eta) = s_0(\eta) + \int_{\Lambda^+} \Delta(\eta, \mu) [s(\eta) - s(\mu)] u(\mu) |d\mu|, \quad (12)$$

where Λ^+ is the two-dimensional compact support of the DOS $u(\eta)$ (defined earlier in Sec. II B) located in the upper half plane \mathbb{C}^+ of the complex spectral plane

$$\Delta(\eta, \mu) = \frac{1}{\text{Im}[R_0(\eta)]} \left[\ln \left| \frac{\mu - \bar{\eta}}{\mu - \eta} \right| + \ln \left| \frac{R_0(\eta)R_0(\mu) + \eta\mu - \delta_0^2}{R_0(\bar{\eta})R_0(\mu) + \bar{\eta}\mu - \delta_0^2} \right| \right].$$
(13)

The integral term in Eq. (12) describes the modification of the tracer breather mean velocity in a gas due to its interaction with other breathers in the gas having a DOS specified by u. The spectral value η in Eq. (12) can be taken outside Λ^+ ; in that case formula (12) describes the mean velocity of a trial TW breather with the eigenvalue η propagating through a breather gas with the DOS supported Λ^+ .

The interaction kernel $\Delta(\eta, \mu)$ given by Eq. (13) describes the position shift arising in a two-breather interaction. We note that the two-breather interactions have been studied in Refs. [50,75] using the IST, where different forms of the expressions for the position shift were obtained. In the Appendix we demonstrate the equivalence of the kernel $\Delta(\eta, \mu)$ given by (13) to the position shift formula obtained for two-breather collisions in previous works.

For a two-component breather gas, the DOS is a superposition of two Dirac δ functions centered at the complex spectral points $\eta^{[j]}$ (j = 1, 2),

$$u(\eta) = \sum_{j=1}^{2} w^{[j]} \delta(\eta - \eta^{[j]}), \tag{14}$$

where $w^{[j]}$ are the weights of the components. For the DOS specified by Eq. (14), Eq. (12) yields the linear system for the gas component velocities $s^{[j]} \equiv s(\eta^{[j]})$ (j=1,2),

$$s^{[1]} = s_0^{[1]} + \frac{\Delta_{1,2} w^{[2]} (s_0^{[1]} - s_0^{[2]})}{1 - (\Delta_{1,2} w^{[2]} + \Delta_{2,1} w^{[1]})},$$

$$s^{[2]} = s_0^{[2]} - \frac{\Delta_{2,1} w^{[1]} (s_0^{[1]} - s_0^{[2]})}{1 - (\Delta_{1,2} w^{[2]} + \Delta_{2,1} w^{[1]})},$$
(15)

where $s_0^{[j]} \equiv s_0(\eta^{[j]})$ (j = 1, 2) and $\Delta_{j,k} = \Delta(\eta^{[j]}, \eta^{[k]})$. In the numerical simulations presented in Sec. III B, we

In the numerical simulations presented in Sec. III B, we will consider an even simpler situation where a single trial breather parametrized by the eigenvalue $\eta^{[1]}$ interacts with a one-component breather gas having its spectral distribution centered in $\eta^{[2]}$. In such a limit $w^{[1]} \rightarrow 0$ and Eqs. (15) reduce

to

$$s^{[1]} = \frac{s_0^{[1]} - \Delta_{1,2} w^{[2]} s_0^{[2]}}{1 - \Delta_{1,2} w^{[2]}},$$

$$s^{[2]} = s_0^{[2]}.$$
 (16)

The validity of Eqs. (16) in the context of the 1D NLSE dynamics (1) will be verified for the PBG, the KMBG, and the ABG in numerical simulations presented in Sec. III B. As a matter of fact, formula (16) can be obtained directly from Eq. (12) by setting $\eta = \eta^{[1]} \notin \Lambda^+$ (the trial breather eigenvalue), and using $u(\mu) = w^{[2]}\delta(\mu - \eta^{[2]})$, $s(\eta_2) = s_0^{[2]}$, where $\eta^{[2]} \in \Lambda^+$.

B. Interactions in one-component breather gases: Comparison between spectral theory and numerical simulations

In the numerical simulations presented in this section, a trial TW breather with the spectral parameter $\eta = \eta^{[1]}$ is propagated through various single-component BGs having their DOS defined by $u(\eta) = w^{[2]}\delta(\eta - \eta^{[2]})$. We define the spectral parameter $\eta^{[2]}$ as $\eta^{[2]} = \alpha i$, with $\alpha = 1$ for the PBG, $\alpha > 1$ for the KMBG, and $\alpha < 1$ for the ABG. Similar to Fig. 1, the spectral portrait of the considered BGs consists of the branch cut (associated with the plane-wave background of unity amplitude) and a cluster of N = 50 spectral points randomly placed in a small square region of width $\delta = 10^{-4}$ centered around $\eta^{[2]}$. The spectral parameter $\eta^{[1]}$ is chosen in such a way that $\text{Re}(\eta^{[1]}) > 0$, which implies that the free trial TW breather has a negative group velocity in the (x, t) plane [see Eq. (11)].

1. Interactions in the Peregrine breather gas

Figure 2 shows a trial Tajiri-Watanabe breather propagating through a PBG. We observe that the trial breather passes through the PBG without change in its group velocity. This confirms the theoretical result established in Ref. [24] that the propagation of a trial TW breather through a PBG is ballistic. This result can be understood at the qualitative level by the fact that the interaction cross section between the trial breather and the individual Peregrine breathers composing the gas is so weak that the propagation of the trial breather is unaffected by the PBG.

2. Interactions in the Kuznetsov-Ma breather gas

Figure 3 shows a trial TW breather propagating through a KMBG. In contrast to Fig. 2, the multiple interactions between the trial breather and the KM breathers composing the KMBG now significantly influence the propagation of the trial breather; see Figs. 3(a) and 3(b) for a comparison between the trajectory of the free Tajiri-Watanabe breather (white dashed lines) and the trajectory followed by the trial breather in the KMBG. As shown in Fig. 3(b), the trial breather acquires a significant space shift each time its trajectory intersects the trajectory of an individual KM breather composing the BG. At the macroscopic scale, this produces a velocity change of the trial breather inside the KMBG. This leads to a spatial shift ΔX in the position of the trial breather which is measurable when the trial breather emerges from the KMBG [see Fig. 3(a)].

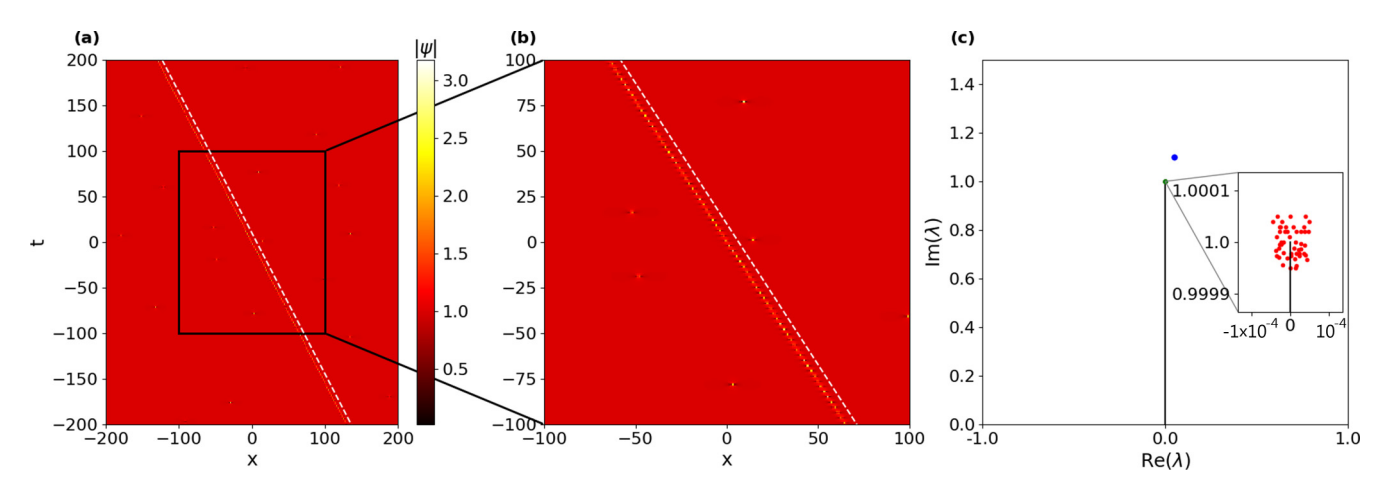


FIG. 2. (a) and (b) Propagation of a Tajiri-Watanabe breather with the spectral parameter $\eta^{[1]} = 0.05 + 1.1i$ inside a Peregrine BG. The space-time evolution shown in (b) represents an enlarged view of the one shown in (a). The white dashed line in (a) and (b) represents the trajectory of the "free" Tajiri-Watanabe breather propagating on a plane-wave background with a group velocity given by Eq. (11). (c) Spectral portrait associated with the numerical results shown in (a) and (b). The vertical line between 0 and +i represents the branch cut associated with the plane-wave background and the blue point is the discrete eigenvalue $\eta^{[1]}$ associated with the Tajiri-Watanabe breather propagating in the PBG. The 50 spectral points characterizing the PBG are densely placed around +i and they are shown in the inset plotted in (c).

For the KMBG, Eq. (16) simplifies to

$$s^{[1]} = \frac{s_0^{[1]}}{1 - \Delta_{1,2} w^{[2]}},\tag{17}$$

given that $s_0^{[2]}=0$. Equation (17) clearly shows that the group velocity of the trial Tajiri-Watanabe breather is increased by a factor $1/(1-\Delta_{1,2}w^{[2]})$ due to the interaction with the KMBG

Note that the space shift ΔX acquired by the trial breather as a result of propagation inside the KMBG simply represents the product of the number N of iterations (equivalently the number of breathers in the KMBG) and the elementary space shift $\Delta_{1,2}$ induced by each interaction: $\Delta X = N\Delta_{1,2}$. This provides an alternative and straightforward way to check the

validity of Eq. (17) which gives the group velocity of the trial breather inside the KMBG.

A set of numerical simulations with different values of the spectral parameters $\eta^{[1]}$ and $\eta^{[2]}$ has been made to check the validity of the spectral theory. Different realizations of the KMBG have been made and the value of $w^{[2]}$ is determined from numerical simulations as the ratio between the selected number N of breathers in the gas over the spatial extension L of the gas: $w^{[2]} = N/L$. As shown in Fig. 4, we observe full quantitative agreement between the numerical experiment and the predictions of the spectral theory.

3. Interactions in the Akhmediev breather gas

The case of the ABG is special and requires separate consideration, particularly because it was not considered in any

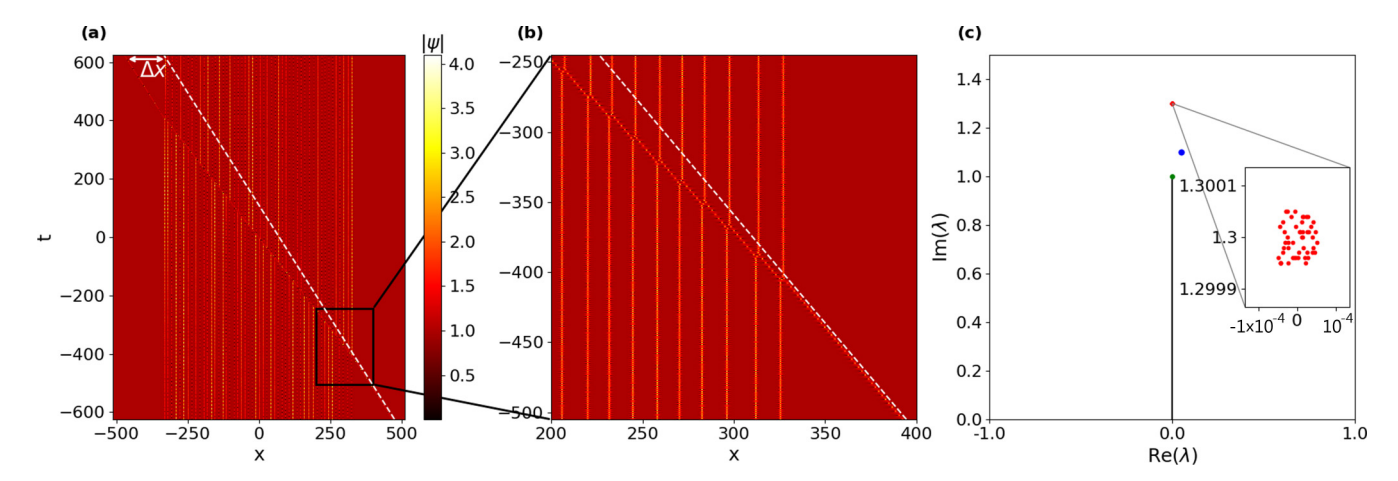


FIG. 3. (a) and (b) Propagation of a TW breather with the spectral parameter $\eta^{[1]} = 0.05 + 1.1i$ inside a Kuznetsov-Ma BG. The space-time evolution shown in (b) represents an enlarged view of the one shown in (a). The white dashed line in (a) and (b) represents the trajectory of the free TW breather propagating on a plane-wave background with a group velocity given by Eq. (11). (c) Spectral portrait associated with the numerical results shown in (a) and (b). The vertical line between 0 and +i represents the branch cut associated with the plane-wave background and the blue point is the discrete eigenvalue $\eta^{[1]}$ associated with the TW breather propagating in the KMBG. The 50 spectral points characterizing the KMBG are densely placed around $\eta^{[2]} = 1.3i$ and they are shown in the inset plotted in (c).

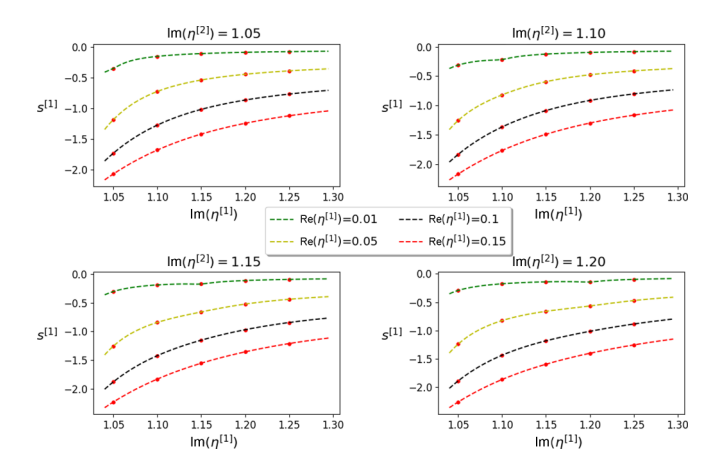


FIG. 4. Quantitative verification of the spectral theory of BGs introduced in Ref. [24]. A comparison is shown between numerics (red dots) and theory (dashed lines) for the effective velocity $s^{[1]}$ of a trial breather $\eta^{[1]}$ propagating in a KMBG $\eta^{[2]}$.

detail in Ref. [24]. The AB is a static object, not localized in space, so it is not immediately obvious how to identify the key quantities $u(\eta)$ and $s(\eta)$ for the ABG. A single AB is a limiting case of the TW breather where the soliton eigenvalue $\eta^{[2]}$ is placed within the branch cut [0, i] in the upper half plane. The ABG is generally characterized by some distribution of soliton eigenvalues along the branch cut. Similar to the above consideration of the KMBG, we consider the ABG with soliton eigenvalues clustered around a given spectral point $\eta^{[2]}$ (and complex conjugate) to mimic a one-component gas.

As we have already mentioned in Sec. III A, the formula (11) for the group velocity of the TW breather implies $|s(\eta)| \to \infty$ as $\eta \to \eta^{[2]}$, which is consistent with the delocalized nature of the AB. On the other hand, it can be shown using the results of Ref. [24] that in the ABG limit the DOS

 $u(\eta) \to 0$ while the spectral flux density function $v(\eta) = s(\eta)u(\eta) = O(1)$. This leads to the alternative form of the equation of state (12),

$$s(\eta) = s_0(\eta) + \int_{\Lambda^+} \Delta(\eta, \mu) \left[\frac{s(\eta)}{s(\mu)} - 1 \right] v(\mu) |d\mu|, \quad (18)$$

which is more suitable for the characterization of the ABG interactions. Equation (18) was obtained from (12) by substituting $u(\eta) = \frac{v(\eta)}{s(\eta)}$. Assuming Λ^+ to be a narrow region surrounding the branch cut [0, i] and using $|s(\mu)| \gg 1$ for $\mu \in \Lambda^+$, Eq. (18) to leading order becomes

$$s(\eta) = s_0(\eta) - \int_{\Lambda^+} \Delta(\eta, \mu) v(\mu) |d\mu|. \tag{19}$$

Equation (19) describes the modification of the velocity of the TW breather with eigenvalue η propagating through the ABG characterized by the spectral flux density $v(\mu)$.

An important property of $\Delta(\eta, \mu)$ given by (13) is that

$$\Delta(\eta, \mu) + \Delta(\eta, -\bar{\mu}) = 0 \quad \text{when } \mu \in [0, i], \tag{20}$$

that is, when μ is on the branch cut [0, i]. The second variable η can take any value in the upper half plane. Equation (20) implies that $\Delta(\eta, \mu)$ takes opposite values on the opposite sides of the branch cut.

It can further be shown that in the case of a breather gas, whose spectral support Λ^+ is symmetric with respect to the branch cut [0, i], the function $v(\eta)$ also takes opposite values on the opposite sides of [0, i]. Thus the speed of the ABG $s(\eta)$ from (18) *does not depend* on which side of the upper part of the branch cut [0, i] the domain Λ^+ or its parts are situated.

Let us now consider a one-component \overline{ABG} with the spectral flux density $v(\eta) = w^t \delta(\eta - \eta^{[2]})$, where $\eta^{[2]} \in [0, i]$ and w^t is a real constant weight. As a result, Eq. (19) assumes a simple form

$$s(\eta) = s_0(\eta) - w^t \Delta(\eta, \eta^{[2]}).$$
 (21)

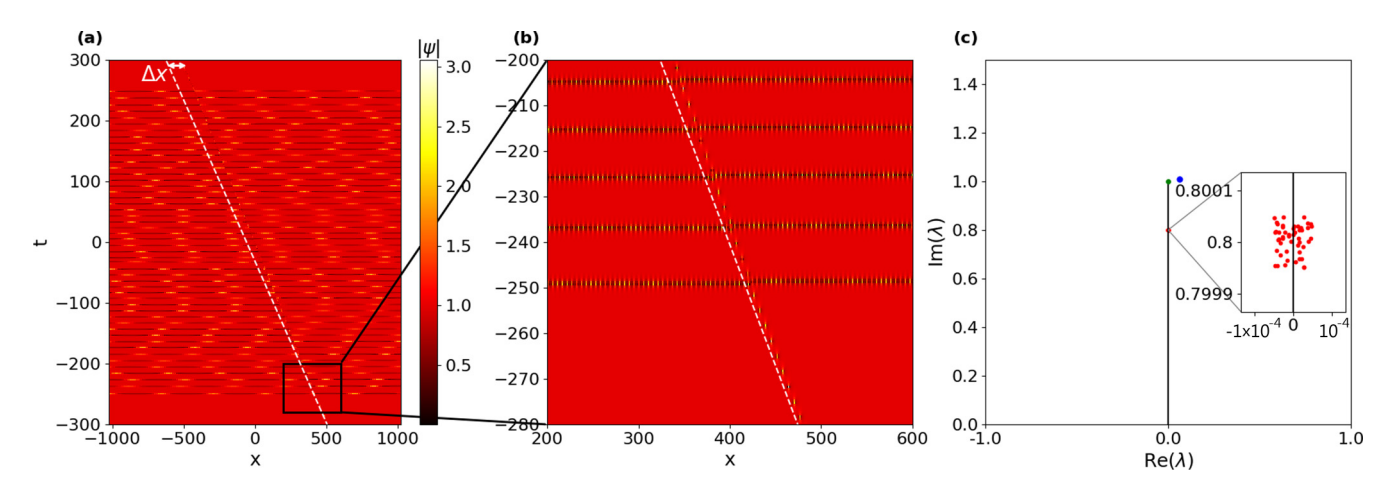


FIG. 5. (a) and (b) Propagation of a TW breather with the spectral parameter $\eta_1 = 0.06 + 1.01i$ inside an Akhmediev BG. The space-time evolution shown in (b) represents an enlarged view of the one shown in (a). The white dashed line in (a) and (b) represents the trajectory of the free TW breather propagating on a plane-wave background with a group velocity given by Eq. (11). (c) Spectral portrait associated with the numerical results shown in (a) and (b). The vertical line between 0 and +i represents the branch cut associated with the plane-wave background and the blue point is the discrete eigenvalue η_1 associated with the TW breather propagating in the ABG. The 50 spectral points characterizing the KMBG are densely placed around $\eta^{[2]} = 0.8i$ and they are shown in the inset plotted in (c).

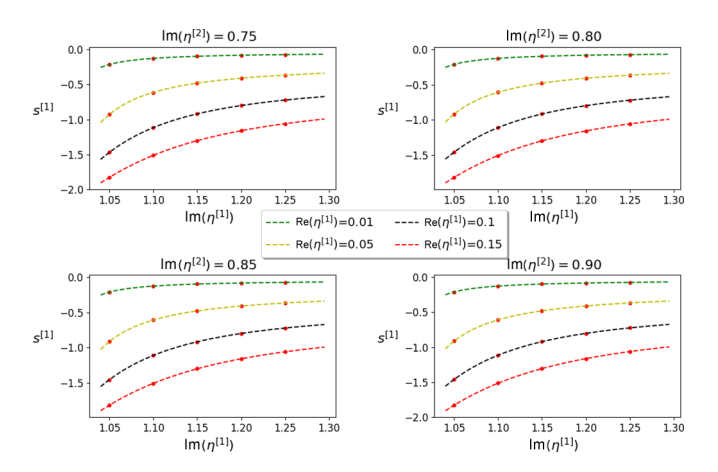


FIG. 6. Comparison between numerics (red dots) and theory (dashed lines) for the effective velocity $s^{[1]}$ of a trial TW breather $\eta^{[1]}$ propagating in an ABG $\eta^{[2]}$.

We note that the sign of w^t , as was explained above, depends on the side of [0, i] but the sign of the product $w^t \Delta$ does not. Hence we have the general result $s(\eta) - s_0(\eta) < 0$ for the propagation of a trial breather through an ABG.

We note that formula (21) can be obtained directly from the basic result (16) by using $w^{[2]} \to 0$ and introducing $w^{[2]} s_0^{[2]} \equiv w^t$. This simple formal consideration, however, does not provide the important information about the sign of $w^t \Delta$.

Figure 5 shows a trial TW breather propagating through an ABG. Similar to Fig. 3, the propagation of the trial breather is significantly influenced by the the multiple interactions with the ABs composing the ABG [see Figs. 5(a) and 5(b)]. One can see that, in contrast to the interaction of the trial TW breather with the KMBG, the group velocity of the trial TW breather is reduced in the interaction with the ABG, in agreement with Eq. (21). Indeed, the space shifts observed in Figs. 3(a) and 5(a) have opposite signs.

Similar to the KMBG interactions, a set of numerical simulations with different values of the spectral parameters $\eta^{[1]}$ and $\eta^{[2]}$ has been made to check the validity of Eq. (21). Different realizations of the ABG have been produced and the value of w^t was determined from numerical simulations as the ratio between the selected number N of ABs in the gas over the temporal extension T of the gas: $w^t = N/T$. As shown in Fig. 6, we observe full quantitative agreement between the numerical experiment and the predictions of the spectral theory.

IV. CONCLUSION

We have developed a numerical algorithm of the IST spectral synthesis of breather gases for the focusing 1D NLS equation. The algorithm is based on the recursive Darboux transform scheme realized in high-precision arithmetics. Using this algorithm, we have synthesized numerically three types of prototypical breather gases: the Akhmediev, Kuznetsov-Ma, and Peregrine gases.

Using the spectral algorithm developed, the interaction properties of breather gases, predicted by the kinetic theory of Ref. [24], have been tested by propagating through them a trial generic TW breather whose effective velocity is strongly

affected by the interaction with the gas. In all cases the theoretically predicted effective mean velocity of the trial breather propagating through a breather gas demonstrates excellent agreement with the results of the numerical simulations. The verification of the theory, despite the inevitable effects of modulational instability present in the 1D NLSE dynamics, has been made possible due to the whole numerical algorithm being based on the spectral construction rather than direct simulations of the 1D NLSE.

The quantitative verification of the kinetic theory of breather gases undertaken in this paper is an important step towards a better understanding of this type of turbulent motion in integrable systems. We also believe that the ability to synthesize numerically BGs represents an important step towards the controlled laboratory generation of BGs, possibly following an approach similar to the one recently reported for hydrodynamic SGs [19]. Finally, the possibility to generate numerically breather solutions of order $N \gtrsim 10$ paves the way for further works devoted to the investigation of the properties of localization in space and time of breather solutions of the 1D NLSE of very high order [38,50,73].

ACKNOWLEDGMENTS

This work was partially supported by the Agence Nationale de la Recherche through the I-SITE ULNE (Grant No. ANR-16-IDEX-0004), the LABEX CEMPI (Grant No. ANR-11- LABX-0007), and the Equipex Flux (Grant No. ANR-11-EQPX-0017), as well as by the Ministry of Higher Education and Research, Hauts de France Council and European Regional Development Fund through the CPER project Photonics for Society (P4S), EPSRC (UK) Grant No. EP/R00515X/2 (G.E.), US NSF Grant No. DMS 2009647 (A.T.), and Dstl (UK) Grant No. DSTLX-1000116851 (G.R., G.E., and S.R.). G.E., A.T., and G.R. thank the PhLAM laboratory at the University of Lille for hospitality and partial financial support.

APPENDIX: POSITION SHIFT IN TWO-BREATHER INTERACTIONS

Two-breather interactions have been studied in Refs. [50,75], where the expressions for the phase and position shifts in the interaction of two Tajiri-Watanabe breathers have been derived using the IST analysis. In Sec. III A the interaction kernel in the equation of state (12) for the breather gas was obtained in the form (13). The natural interpretation of this interaction kernel, consistent with the previously studied cases of KdV and NLS soliton gases, is the position shift in a two-breather collision. However, the equivalence between formula (13) and the expressions from [50,75] is far from obvious. Here we establish this equivalence, enabling one to extend the phenomenological interpretation of soliton gas kinetics [23] to breather gases.

We consider the position shift expression from [75],

$$\Delta \bar{\xi}_2 = -\ln(\xi_0)/c_{-2}\cos\alpha_2 = \Delta(\lambda_2, \lambda_1), \quad (A1)$$

where

$$\xi_0 = \frac{d_+ - 2[\cos(\alpha_1 - \alpha_2) + c_{-,1}c_{-,2}]\cos(\alpha_1 - \alpha_2)}{d_+ - 2[\cos(\alpha_1 + \alpha_2) - c_{-,1}c_{-,2}]\cos(\alpha_1 + \alpha_2)}, \quad (A2)$$

with

$$c_{\pm,j} = z_j \pm q_0^2/z_j, \quad \lambda_j = (\zeta_j - q_0^2/\zeta_j)/2,$$

$$d_{\pm,j} = z_j^2 \pm q_0^4/z_j^2, \quad q_0 = -i\delta_0,$$

$$d_+ = d_{+,1} + d_{+,2}, \quad R_0(\lambda_j) = (\zeta_j + q_0^2/\zeta_j)/2,$$

$$\zeta_j = R_0(\lambda_j) + \lambda_j = iz_j e^{i\alpha_j}.$$
(A3)

One can verify that substituting (A3) in Eq. (13) and invoking the identities

$$|\lambda_{i}|^{2} = \left(d_{+,i} + 2q_{0}^{2}\cos\alpha_{i}\right)/4,$$

$$d_{+} = \left(z_{1}z_{2} + \frac{q_{0}^{4}}{z_{1}z_{2}}\right)\left(\frac{z_{1}}{z_{2}} + \frac{z_{2}}{z_{1}}\right),$$

$$(\cos 2\alpha_{1} + \cos 2\alpha_{2})/2 = \cos\alpha_{1} + \alpha_{2}\cos\alpha_{1} - \alpha_{2}$$
(A4)

yields the position shift expression (A1).

- [1] S. P. Novikov, S. V. Manakov, L. P. Pitaevskii, and V. E. Zakharov, *Theory of Solitons: The Inverse Scattering Method* (Springer Science + Business Media, New York, 1984).
- [2] V. E. Zakharov, Turbulence in integrable systems, Stud. Appl. Math. 122, 219 (2009).
- [3] M. D. Maiden, D. V. Anderson, N. A. Franco, G. A. El, and M. A. Hoefer, Solitonic Dispersive Hydrodynamics: Theory and Observation, Phys. Rev. Lett. 120, 144101 (2018).
- [4] G. A. El and M. A. Hoefer, Dispersive shock waves and modulation theory, Physica D 333, 11 (2016).
- [5] A. A. Gelash and V. E. Zakharov, Superregular solitonic solutions: A novel scenario for the nonlinear stage of modulation instability, Nonlinearity 27, R1 (2014).
- [6] B. Kibler, A. Chabchoub, A. Gelash, N. Akhmediev, and V. E. Zakharov, Superregular Breathers in Optics and Hydrodynamics: Omnipresent Modulation Instability Beyond Simple Periodicity, Phys. Rev. X 5, 041026 (2015).
- [7] G. Xu, A. Gelash, A. Chabchoub, V. Zakharov, and B. Kibler, Breather Wave Molecules, Phys. Rev. Lett. 122, 084101 (2019).
- [8] J. M. Soto-Crespo, N. Devine, and N. Akhmediev, Integrable Turbulence and Rogue Waves: Breathers or Solitons? Phys. Rev. Lett. 116, 103901 (2016).
- [9] N. Akhmediev, J. M. Soto-Crespo, and N. Devine, Breather turbulence versus soliton turbulence: Rogue waves, probability density functions, and spectral features, Phys. Rev. E 94, 022212 (2016).
- [10] S. Randoux, P. Walczak, M. Onorato, and P. Suret, Intermittency in Integrable Turbulence, Phys. Rev. Lett. 113, 113902 (2014).
- [11] P. Walczak, S. Randoux, and P. Suret, Optical Rogue Waves in Integrable Turbulence, Phys. Rev. Lett. **114**, 143903 (2015).
- [12] P. Suret, R. El Koussaifi, A. Tikan, C. Evain, S. Randoux, C. Szwaj, and S. Bielawski, Single-shot observation of optical rogue waves in integrable turbulence using time microscopy, Nat. Commun. 7, 13136 (2016).
- [13] G. Michel, F. Bonnefoy, G. Ducrozet, G. Prabhudesai, A. Cazaubiel, F. Copie, A. Tikan, P. Suret, S. Randoux, and E. Falcon, Emergence of peregrine solitons in integrable turbulence of deep water gravity waves, Phys. Rev. Fluids 5, 082801(R) (2020).
- [14] A. Costa, A. R. Osborne, D. T. Resio, S. Alessio, E. Chrivì, E. Saggese, K. Bellomo, and C. E. Long, Soliton Turbulence in Shallow Water Ocean Surface Waves, Phys. Rev. Lett. 113, 108501 (2014).
- [15] J. Wang, Q. W. Ma, S. Yan, and A. Chabchoub, Breather Rogue Waves in Random Seas, Phys. Rev. Appl. 9, 014016 (2018).

- [16] A. R. Osborne, D. T. Resio, A. Costa, S. Ponce de Leòn, and E. Chirivì, Highly nonlinear wind waves in Currituck Sound: Dense breather turbulence in random ocean waves, Ocean Dyn. 69, 187 (2019).
- [17] A. R. Osborne, Breather turbulence: Exact spectral and stochastic solutions of the nonlinear Schrödinger equation, Fluids 4, 72 (2019).
- [18] I. Redor, E. Barthélemy, H. Michallet, M. Onorato, and N. Mordant, Experimental Evidence of a Hydrodynamic Soliton Gas, Phys. Rev. Lett. 122, 214502 (2019).
- [19] P. Suret, A. Tikan, F. Bonnefoy, F. Copie, G. Ducrozet, A. Gelash, G. Prabhudesai, G. Michel, A. Cazaubiel, E. Falcon, G. El, and S. Randoux, Nonlinear Spectral Synthesis of Soliton Gas in Deep-Water Surface Gravity Waves, Phys. Rev. Lett. 125, 264101 (2020).
- [20] A. Gelash, D. Agafontsev, V. Zakharov, G. El, S. Randoux, and P. Suret, Bound State Soliton Gas Dynamics Underlying the Spontaneous Modulational Instability, Phys. Rev. Lett. 123, 234102 (2019).
- [21] V. E. Zakharov, Kinetic equation for solitons, Sov. Phys.—JETP **33**, 538 (1971).
- [22] G. A. El, The thermodynamic limit of the Whitham equations, Phys. Lett. A 311, 374 (2003).
- [23] G. A. El and A. M. Kamchatnov, Kinetic Equation for a Dense Soliton Gas, Phys. Rev. Lett. 95, 204101 (2005).
- [24] G. El and A. Tovbis, Spectral theory of soliton and breather gases for the focusing nonlinear Schrödinger equation, Phys. Rev. E **101**, 052207 (2020).
- [25] N. Akhmediev, A. Ankiewicz, and J. M. Soto-Crespo, Rogue waves and rational solutions of the nonlinear Schrödinger equation, Phys. Rev. E 80, 026601 (2009).
- [26] N. Akhmediev, A. Ankiewicz, and M. Taki, Waves that appear from nowhere and disappear without a trace, Phys. Lett. A 373, 675 (2009).
- [27] D. J. Kedziora, A. Ankiewicz, and N. Akhmediev, Second-order nonlinear Schrödinger equation breather solutions in the degenerate and rogue wave limits, Phys. Rev. E **85**, 066601 (2012).
- [28] G. Genty, C. M. de Sterke, O. Bang, F. Dias, N. Akhmediev, and J. M. Dudley, Collisions and turbulence in optical rogue wave formation, Phys. Lett. A 374, 989 (2010).
- [29] J. M. Dudley, G. Genty, A. Mussot, A. Chabchoub, and F. Dias, Rogue waves and analogies in optics and oceanography, Nat. Rev. Phys. 1, 675 (2019).
- [30] E. A. Kuznetsov, On solitons in parametrically unstable plasma, Akad. Nauk SSSR Dokl. **236**, 575 (1977).
- [31] D. H. Peregrine, Water waves, nonlinear Schrödinger equations and their solutions, J. Aust. Math. Soc. B 25, 16 (1983).

- [32] N. N. Akhmediev and V. I. Korneev, Modulation instability and periodic solutions of the nonlinear Schrödinger equation, Theor. Math. Phys. 69, 1089 (1986).
- [33] B. Kibler, J. Fatome, C. Finot, G. Millot, F. Dias, G. Genty, N. Akhmediev, and J. M. Dudley, The Peregrine soliton in nonlinear fibre optics, Nat. Phys. 6, 790 (2010).
- [34] A. Chabchoub, N. P. Hoffmann, and N. Akhmediev, Rogue Wave Observation in a Water Wave Tank, Phys. Rev. Lett. 106, 204502 (2011).
- [35] S. Randoux, P. Suret, and G. El, Inverse scattering transform analysis of rogue waves using local periodization procedure, Sci. Rep. 6, 29238 (2016).
- [36] M. Tajiri and Y. Watanabe, Breather solutions to the focusing nonlinear Schrödinger equation, Phys. Rev. E 57, 3510 (1998).
- [37] N. N. Akhmediev, V. I. Korneev, and N. V. Mitskevich, *N*-modulation signals in a single-mode optical waveguide under nonlinear conditions, Sov. Phys.—JETP 67, 89 (1988).
- [38] D. J. Kedziora, A. Ankiewicz, and N. Akhmediev, Classifying the hierarchy of nonlinear-Schrödinger-equation rogue-wave solutions, Phys. Rev. E 88, 013207 (2013).
- [39] A. A. Gelash and D. S. Agafontsev, Strongly interacting soliton gas and formation of rogue waves, Phys. Rev. E 98, 042210 (2018).
- [40] V. E. Zakharov and A. B. Shabat, Exact theory of two-dimensional self-focusing and one-dimensional selfmodulation of waves in nonlinear media, Sov. Phys.—JETP 34, 62 (1972).
- [41] J. Yang, *Nonlinear Waves in Integrable and Non-Integrable Systems* (Society for Industrial and Applied Mathematics, Philadelphia, PA, USA, 2010).
- [42] S. Wahls and H. V. Poor, Fast numerical nonlinear fourier transforms, IEEE Trans. Inf. Theory 61, 6957 (2015).
- [43] S. T. Le, V. Aref, and H. Buelow, Nonlinear signal multiplexing for communication beyond the Kerr nonlinearity limit, Nat. Photon. 11, 570 (2017).
- [44] S. K. Turitsyn, J. E. Prilepsky, S. T. Le, S. Wahls, L. L. Frumin, M. Kamalian, and S. A. Derevyanko, Nonlinear fourier transform for optical data processing and transmission: Advances and perspectives, Optica 4, 307 (2017).
- [45] Y.-H. Sun, Soliton synchronization in the focusing nonlinear Schrödinger equation, Phys. Rev. E 93, 052222 (2016).
- [46] G. Biondini and G. Kovačič, Inverse scattering transform for the focusing nonlinear Schrödinger equation with nonzero boundary conditions, J. Math. Phys. 55, 031506 (2014).
- [47] G. Biondini and E. Fagerstrom, The integrable nature of modulational instability, SIAM J. Appl. Math. **75**, 136 (2015).
- [48] Y.-C. Ma, The perturbed plane-wave solutions of the cubic Schrödinger equation, Stud. Appl. Math. **60**, 43 (1979).
- [49] V. E. Zakharov and A. A. Gelash, Nonlinear Stage of Modulation Instability, Phys. Rev. Lett. 111, 054101 (2013).
- [50] A. A. Gelash, Formation of rogue waves from a locally perturbed condensate, Phys. Rev. E 97, 022208 (2018).
- [51] A. Chabchoub, N. Hoffmann, M. Onorato, and N. Akhmediev, Super Rogue Waves: Observation of a Higher-Order Breather in Water Waves, Phys. Rev. X 2, 011015 (2012).
- [52] A. Chabchoub, N. Hoffmann, M. Onorato, A. Slunyaev, A. Sergeeva, E. Pelinovsky, and N. Akhmediev, Observation of a

- hierarchy of up to fifth-order rogue waves in a water tank, Phys. Rev. E **86**, 056601 (2012).
- [53] B. Frisquet, B. Kibler, and G. Millot, Collision of Akhmediev Breathers in Nonlinear Fiber Optics, Phys. Rev. X 3, 041032 (2013).
- [54] B. Kibler, J. Fatome, C. Finot, G. Millot, G. Genty, B. Wetzel, N. Akhmediev, F. Dias, and J. M. Dudley, Observation of Kuznetsov-Ma soliton dynamics in optical fibre, Sci. Rep. 2, 463 (2012).
- [55] J. M. Dudley, G. Genty, F. Dias, B. Kibler, and N. Akhmediev, Modulation instability, Akhmediev breathers and continuous wave supercontinuum generation, Opt. Express 17, 21497 (2009).
- [56] J.-W. Goossens, H. Hafermann, and Y. Jaouën, Experimental realization of Fermi-Pasta-Ulam-Tsingou recurrence in a long-haul optical fiber transmission system, Sci. Rep. 9, 18467 (2019).
- [57] D. Luo, Y. Jin, J. H. V. Nguyen, B. A. Malomed, O. V. Marchukov, V. A. Yurovsky, V. Dunjko, M. Olshanii, and R. G. Hulet, Creation and Characterization of Matter-Wave Breathers, Phys. Rev. Lett. 125, 183902 (2020).
- [58] G. Dematteis, T. Grafke, M. Onorato, and E. Vanden-Eijnden, Experimental Evidence of Hydrodynamic Instantons: The Universal Route to Rogue Waves, Phys. Rev. X 9, 041057 (2019).
- [59] P. Dubard, P. Gaillard, C. Klein, and V. B. Matveev, On multirogue wave solutions of the NLS equation and positon solutions of the KdV equation, Eur. Phys. J.: Spec. Top. 185, 247 (2010).
- [60] P. Dubard and V. B. Matveev, Multi-rogue waves solutions to the focusing NLS equation and the KP-I equation, Nat. Hazards Earth Syst. Sci. 11, 667 (2011).
- [61] P. Gaillard, Families of quasi-rational solutions of the NLS equation and multi-rogue waves, J. Phys. A: Math. Theor. 44, 435204 (2011).
- [62] A. Ankiewicz, D. J. Kedziora, and N. Akhmediev, Rogue wave triplets, Phys. Lett. A **375**, 2782 (2011).
- [63] Y. Ohta and J. Yang, General high-order rogue waves and their dynamics in the nonlinear Schrödinger equation, Proc. R. Soc. A 468, 1716 (2012).
- [64] J. S. He, H. R. Zhang, L. H. Wang, K. Porsezian, and A. S. Fokas, Generating mechanism for higher-order rogue waves, Phys. Rev. E **87**, 052914 (2013).
- [65] W.-R. Sun, L. Liu, and P. G. Kevrekidis, Rogue waves of ultrahigh peak amplitude: A mechanism for reaching up to thousand times the background level, Proc. R. Soc. A 477, 20200842 (2021).
- [66] C. Gu, H. Hu, and Z. Zhou, *Darboux Transformations in Integrable Systems: Theory and their Applications to Geometry* (Springer Netherlands, Dordrecht, 2005), pp. 1–64.
- [67] N. N. Akhmediev and N. V. Mitzkevich, Extremely high degree of N-soliton pulse compression in an optical fiber, IEEE J. Quantum Electron. 27, 849 (1991).
- [68] N. Akhmediev, J. M. Soto-Crespo, and A. Ankiewicz, Extreme waves that appear from nowhere: On the nature of rogue waves, Phys. Lett. A 373, 2137 (2009).
- [69] B. Guo, L. Ling, and Q. P. Liu, Nonlinear Schrödinger equation: Generalized Darboux transformation and rogue wave solutions, Phys. Rev. E 85, 026607 (2012).

- [70] F. J. García-Gómez and V. Aref, Statistics of the nonlinear discrete spectrum of a noisy pulse, J. Lightwave Technol. 37, 3563 (2019).
- [71] D. J. Kedziora, A. Ankiewicz, and N. Akhmediev, Circular rogue wave clusters, Phys. Rev. E **84**, 056611 (2011).
- [72] B. M. and A. Tovbis, Maximal amplitudes of finite-gap solutions for the focusing nonlinear Schrödinger equation, Commun. Math. Phys. **354**, 525 (2017).
- [73] B. Yang and J. Yang, Rogue wave patterns in the nonlinear Schrödinger equation, arXiv:2101.00383.
- [74] I. M. Lifshits, S. A. Gredeskul, and L. A. Pastur, *Introduction to the Theory of Disordered Systems* (Wiley, New York, 1988).
- [75] S. Li and G. Biondini, Soliton interactions and degenerate soliton complexes for the focusing nonlinear Schrödinger equation with nonzero background, Eur. Phys. J. Plus 133, 400 (2018).